2018-01-01

An Integrated Machine Learning Geological Field Tool In The Age Of Big Data And Drones

Guillermo Vargas
University of Texas at El Paso, gavargas22@gmail.com

AN INTEGRATED MACHINE LEARNING GEOLOGICAL FIELD TOOL IN THE AGE OF BIG DATA AND DRONES

GUILLERMO VARGAS

Master's Program in Program in Geophysics

APPROVED:

Laura Serpa, Ph.D., Chair

Jose Miguel Hurtado, Jr., Ph.D.

Steven Varela, M.A

Charles Ambler, Ph.D.
Dean of the Graduate School

AN INTEGRATED MACHINE LEARNING GEOLOGICAL FIELD TOOL IN THE AGE OF BIG DATA AND DRONES

by

GUILLERMO VARGAS, B.S.

THESIS

Presented to the Faculty of the Graduate School of

The University of Texas at El Paso

in Partial Fulfillment

of the Requirements

for the Degree of

MASTER OF SCIENCE

Department of Geological Sciences

THE UNIVERSITY OF TEXAS AT EL PASO
December 2018

ACKNOWLEDGMENTS

I would like to thank Dr. Laura Serpa for always believing in me and for being so understanding of life's difficulties, and for all the help you provided to me in my long college career, I am forever in debt to you. I want to thank Dr. Jose Hurtado for being tough and teaching me remote sensing and professionalism. I would like to thank Mayra Guerrero for being with me in the field collecting data with the drone and having conversations while driving hours and hours to the field areas. I want to thank Alfredo Rojo for being with me in the field and being a great friend. Xiao Wei Li who taught me so much about geology. Matthew Fox for being a very good friend and helping me become a better person and better geologist. Matthew Hiebing for being a good friend. I would like to thank Felix Ramirez, for being there to advise me with all his professional experience and being a great friend. I would like to thank Ralph Delfin for helping me out flying the drone and being a great friend. Many thanks for the whole Indios crew, Andy Anderson, in some way they all contributed to this project small as it might be. So many other people that even though did not work in my project directly. Forged my experience and memory of college that I will never forget.

I want to thank my mother Patty; her bravery and exemplary life gave me the values and mindset that help me to go through everything life throws at me. I want to thank my wife Jean for supporting me and providing me with the inspiration to push through and become a better man. I am thankful to God who gave me this life I now live and brought my beautiful daughter Irene to this world.

It has been a great few years in college, and now it's time to grow up and become a productive member of society in this beautiful country, the United States of America.

ABSTRACT

Unmanned aerial vehicles (UAVs) and machine learning are relatively new research tools in the geosciences that can be used to collect and analyze large data sets rapidly. We combine the power of rapid data collection using unmanned aerial vehicles with machine learning algorithms to develop a field-based system to identify targeted geological features. For data collection, we have used a commercial-grade UAV which carried visible-wavelength and multispectral (visible-infrared) cameras. We analyzed the data with machine learning and machine vision algorithms that can classify rock units exposed in a field area. We have identified algorithms that in previous literature have proven to be reliable in predicting characteristics. These include k-Nearest Neighbors, Support Vector Machines, K-Means Clustering and Convolutional Neural Networks which we tested to determine their effectiveness in geologic mapping. Several filtering operations were applied to the collected imagery. K-Means clustering was used to generate some preliminary segmentation of lithology on the ground. We then ran 3 supervised machine learning algorithms and the results were field tested to determine how they compared to a professional grade geologic map. The results show that consumer-grade machine learning algorithms and consumer-grade UAV platforms can be integrated into a package that can act as a field assistant and generate preliminary geologic maps. The accuracy results of the algorithms were tested by employing a test/train split of the labeled dataset. The highest accuracy reported was for the SVM algorithm with an accuracy reported of 76% in the classification of 2 visually distinct rock units. We have also shown that by introducing Kuwahara and Median filters, normally used in computer vision applications, we can reduce effects of vegetation and increase the prediction accuracy.

TABLE OF CONTENTS

LIST OF FIGURES

INTRODUCTION

Over the past decade, unmanned aerial vehicles (UAVs) have found many uses in the geological sciences. Structure from motion (SfM) photogrammetry and the production of aerial orthoimagery are some of the applications that have been especially useful (Westoby, 2012). Through these and other methods, UAVs have become a very reliable means of obtaining geologically-relevant aerial image data rapidly and at a high spatial resolution. The types of data that UAVs can gather, and the rate at which UAVs can gather that data, are similar to satellite imaging systems, this has the potential to make geologic models and geologic analysis more accurate by providing more data points and observations with which to create more detailed geologic models and predictions (D'Alessandro, 2015). UAVs have produced an increase in data availability and it has produced a growing need for processing that data. The sheer quantity of data available poses a challenge, and, as a result, many data analysis software tools have been developed such as K-Means Clustering, Support Vector Machines, and Artificial Neural Networks.

One area of data analysis software development is machine learning, where a computer program is provided a large data set and algorithms can be trained to make decisions or predictions without being specifically programmed to do so (REF). Machine learning is being used successfully in many scientific and industrial applications. The geosciences can gain a lot from machine learning due to the large amounts of data produced in a geologic study. Here we present the results of applying a combination of UAV data collection with and machine learning algorithms to accomplish fully autonomous geologic mapping of a field site in west Texas.

Geologic mapping is one of the principal components of field geology. A geologic map is a 2D graphical representation of the spatial distribution of rock units on the surface of the earth. The information contained in a geologic map is useful for gaining understanding of the stratigraphy,

structure, and geologic history of an area, including making predictions of the subsurface geology. As such it can be very useful scientifically as well as economically, for example, in prospecting and extracting economically valuable materials (Bolton, 1989). However, a good quality geologic map requires a lot of work to create on the part of a field geologist. Geologic maps may demand extensive and expensive field data collection campaigns requiring substantial time in the field on the part of the field geologist. The very time-consuming task of obtaining field data has not fundamentally changed until recent years, and, only recently, have digital tools begun to replace the traditional "paper and pencil" field mapping (Pavlis, 2011). The geosciences are slowly adapting new digital techniques for geologic mapping, and these tools, such as UAVs, have started a revolution in field data collection (Pavlis & Mason, 2017).

2. BACKGROUND

2.1 Unmanned Aerial Vehicles (UAVs) in the Geosciences

UAVs and machine learning are highly researched topics, and a large number of papers are available related to these subjects. In UAVs we have structure from motion (Carceroni et al., 2006), machine learning aided satellite image recognition (Cracknell et al., 2014), applications of drones to geophysics (D'Alessandro, 2015), and low cost drone applications in structural geology (Westoby, 2012). In other words, many scientists have recognized the potential of UAVs in geosciences. UAVs are now widely used in the extraction of data to generate 3D models of geologic structures through Structure from Motion (Pavlis & Mason, 2017), vegetation studies, photogrammetry, and three-dimensional geologic modelling of geologic structures. For example, Vázquez-Tarrío (2017) obtained imagery from an UAV to generate a 3D model that assisted in the characterization of grain size in gravel bars in braided rivers. Machine learning has also been applied to satellite remotely sensed imagery to detect the presence of rocks associated with economically valuable minerals (Cracknell, 2014).

2.2 Machine Learning

Over the past three decades, machine learning has become an important tool in fields such as optical character recognition, and autonomous vehicles. There are algorithms that calculate the fastest route through a maze of roads, predict the structure of proteins, and automatically classify of celestial objects, among many other applications (Turk, 1991; Langley et al., 1995). Machine learning has been used in geoscience studies to map land cover types, monitor land usage, and perform vegetation classification (Cracknell et al., 2014). Some work has been done in the field of

identifying and classifying lithologies of economically valuable minerals, primarily with unsupervised machine learning algorithms (Cracknell et al., 2014).

Renguang et al. (2011) used the support vector machines (SVM) algorithm to identify the mineral viability of gold deposits in Nova Scotia. The resulting classifications led to 5-9% fewer total errors as compared with a weights-of-evidence method that does not use machine learning. Renguang et al. used four features to describe the concentration of potential of gold deposits: (1) optimum proximity to an anticline structure; (2) contact between the Hallifax and Goldenville formations which often appear in economically valuable deposits; and (3) geochemical composition background values. This collection of data allowed for the creation of a feature vector, which is a representation of all the attributes that describe an observed feature (Langley et al., 1995). Renguang et al. trained the SVM algorithm to recognize known prospect areas with close to 100% accuracy. The SVM algorithm identified other potential prospect areas with a false positive rate of 32.6%, although the algorithm may have been overfitted. Renguang et al. showed the power of machine learning algorithms to help in identification of rock units; furthermore, showed the steps necessary to execute a machine learning algorithm-based analysis of a geologic problem.

Petropoulos et al. (2012) describes the process of processing hyperspectral imagery for machine learning use. They implemented SVM and artificial neural networks (ANN) classifiers for discriminating land-cover classes. They found that both algorithms were useful for classifying land cover and that the two algorithms have a very similar classification accuracy, with SVM outperforming ANN by ~3%. Petropoulos et al. applied an atmospheric correction to the input images and computed the principal components of the images. Training points were chosen carefully by Petropoulos et al. from known land cover types, previously known land cover types

were then used as labels for the training data set. This dataset was then later fed into the algorithms. The result was a trained algorithm that could identify multiple land cover classes with accuracies ranging from 68% to 100%. The techniques described by Petropoulos et al. to train MLAs could be easily adapted for the task of identifying rock units.

New developments in machine learning have resulted in a new type of machine learning algorithm that uses many layers of artificial neural networks (LeCun, 2017). These new, "deep learning" algorithms have proven to be the most promising image classification algorithms to date (Krizhevsky, 2012). Convolutional neural networks (CNNs), which are a type of deep machine learning, have shown high performance in analysis of visual imagery (LeCun, 2017). Kussul, et al. (2017), for example, have employed deep learning methods to detect land cover types and to perform crop type classification. Using Google's TensorFlow Deep Learning Framework (https://www.tensorflow.org/), Kussul et al. used multispectral imagery from Landsat-8 and synthetic aperture radar data from Sentinel-1. After preprocessing of the data obtained from the satellites, the training step of the CNN took about 12 hours to train, the result was an algorithm that could identify land cover and crop types in a satellite image (Kussul, et al., 2017).

All the previously mentioned papers in this section show that machine learning algorithms, can be used to interpret large quantities of geoscience-related data, specifically data collected by a satellite, but the work and techniques could be applied to data collected by UAVs. The work provided a blueprint for how the experiments in this paper could be conducted.

2.2.1 Supervised Machine Learning

The first step to understand machine learning is to become familiar with the various kinds of algorithms. One algorithm type is supervised machine learning. Supervised machine learning includes classification and pattern recognition algorithms that utilize training data that are produced manually by a person who can recognize the pattern being sought. For this project, three supervised machine learning algorithms that have been used successfully in other mapping applications (Cracknell M. J., et al, 2014) were considered. We will now go through some of the key concepts in machine learning.

2.2.1.1 What is a Feature Vector?

When a geologic observation is conducted, a geologist will often use specific vocabulary, measurements, and descriptions to describe an observation. For example, say a geologist is walking on the field creating a geologic map, and encounter a rock unit which has not been previously mapped. A description may look like this: "*Tan to light gray, medium grained, sandstone with interbedded shales, fossiliferous with a strike and dip of 130/19 East".* This is a description of the color, grain size, clastic composition, and its tendency to dip 19 degrees east and strike 130 degrees. This is then processed in the geologists' brain and is used for identification later if the rock unit is encountered again. That geologist's description becomes what describes an observation, which can be communicated to other geologists and can be used to identify the rock unit in the future.

How would we be able to tell a computer program the information those parameters describe *that* rock unit? This is where the feature vector comes in. The data in the description,

could be converted into numerical information. For example, we could generate a matrix that contains all the observations, quantified.

This becomes a feature vector that the computer can use to identify a specific rock unit, because of the characteristics contained in the vector.

Red	Green	Blue	Hue	Saturation	Value	Label
0.31	0.57	0.82	0.63	0.85	0.2	0
0.87	0.21	0.36	0.45	0.32	0.87	1

2.2.1.2 Data Set Balancing

In the age of big data, we have an abundance of data points from multiple sensors, and the rate at which data collected can be massive as technologies improve. In order to make sense of all this data, MLAs can be used. The more data available the better an MLA might work, but there is a caveat, called the "curse of dimensionality". Each observation from a different sensor is a dimension added to a data set, which can contain too many observations of a classification and much less of another classification. This causes a tendency of MLAs to become too eager to classify points as the label that the majority of points in a dataset have. In order to mitigate this problem, a dataset decimation is necessary. This operation involves the deletion of data points of the over-represented labels and bringing the distribution of labels to be equal to the classification that has the least number of occurrences.

2.2.1.3 K-Nearest Neighbor (KNN) Classification

The K-Nearest neighbor (KNN) supervised machine learning algorithm works by analyzing the neighborhood of any data point in a dataset. We will assume that the data being analyzed in this example is an image. The KNN algorithm essentially functions as majority vote operation within the neighborhood of every analyzed pixel. Every single pixel is observed individually, and the algorithm observes what the classification of the majority of the surrounding labeled pixels is and assigns that classification to the pixel being observed (Altman, 1992). This type of classification has been proposed and used for many years as an automated classification method in applications ranging from facial recognition, handwritten character identification. The algorithm is often used as a baseline, to compare any other algorithm and how much more effective they are in comparison (Cover et al., 1967). One of its advantages is that training time is greatly reduced in comparison to other more computationally expensive algorithms such as SVM and CNN (which will be explored later in this chapter) because the algorithm doses not adjust its parameters to fit a mathematical model, but, instead it uses labeled data points in a training set to classify unknowns (Cover et al., 1967). Among the disadvantages is that the KNN algorithm can overfit quickly and produce false positive results, in other words the algorithm is susceptible to become over confident in classifying data points, it will become too eager to assign an overfitted category to unknowns. This is especially the case when a training data set has not been balanced, by having the same number of labels for each class. If a majority of the values in a feature vector have large magnitudes the algorithm may become biased towards the higher weight features. Another issue with the KNN algorithm is that if any one of the classes being considered amounts to a very large percentage of the total data set, the algorithm will overfit to this class. For this reason, the dataset needs to be

balanced (Coomans et al., 1982). Overall though, the KNN algorithm is very easy to use and provides a baseline of performance of an algorithm.

2.2.1.4 Support Vector Machine (SVM) Classification

Machine learning can also be a general mathematical function approximator that uses polynomial regression and curve fitting to learn from data (REF). One machine learning algorithm that has been used successfully for geoscience applications is the Support Vector Machine

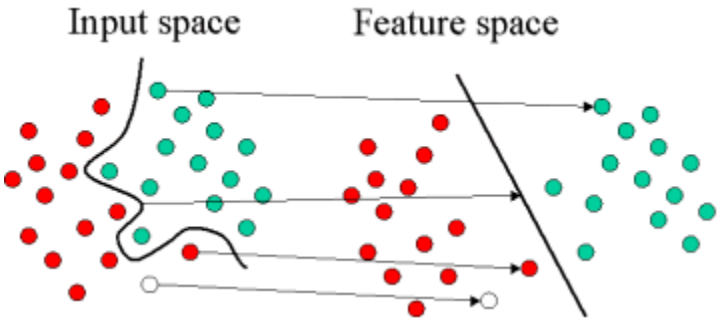

Figure 2. 1 A hyperplane generated in a two-dimensional dataset that separates the green and red dots, as seen in the input space and feature space, where an optimal separation plane was found (from http://www.statsoft.com/textbook/support-vector-machines).

algorithm (SVM) (Cracknell et al., 2014). SVM separates data points in high-dimensional space by using a hyper-dimensional plane. For example, if one has a large collection of 2-D points they can be plotted in a two-dimensional plane. The SVM algorithm uses curve fitting and generates a curve that most optimally separates the different points in the data set. Figure 1 shows a two-dimensional representation of the curve separating distribution of green and red points by a curve which the SVM algorithm arrived at mathematically.

2.2.1.5 Convolutional Neural Networks (CNN)

Convolutional Neural Networks (CNNs) are a type of multi-layered Artificial Neural Networks and are one of the latest developments in the field of machine learning. They employ multiple advances in machine learning and biological cognitive science (Matsugu et al., 2003). These algorithms have sparked a revolution in machine vision. They are being used in commercial grade self-driving cars, (Bojarski, et al., 2017) recognition of images by web services like Amazon and Google (Koehrsen, 2017). Most applications of CNNs are in machine vision, but other applications include tasks such as natural language processing. CNN algorithms yield better results in machine vision tasks when compared to other algorithms such as KNN and SVM at the cost of more computational expense. One of their main advantages is that CNN algorithms generally require fewer filtering operations, preprocessing, and feature extraction than any other computer vision algorithm such as SVM. In the example of a self-driving car, whereas other types of MLAs require traffic lanes to be first highlighted in imagery with an edge detection filter, CNNs are capable of ingesting raw imagery, deducing filters that can extract features such as traffic lanes automatically, the convolutional neural network learns the filters and conducts feature extraction on its own. This would have to be hard coded into the workflow with other algorithms (Cornelisse, 2018).

2.2.2 Unsupervised Machine Learning

We tested the classification abilities of one unsupervised machine learning algorithm which did not need any training data to set up. The input can be the raw data and the algorithm can detect patterns in data. This kind of algorithm is normally employed when there is no readily available labeled data and can be used in combination with supervised algorithms to reduce the number of measurements that the computer has to analyze and make the process more efficient.

2.2.2.1 K-Means Clustering Classification

K-Means clustering organizes randomized data points into clusters by continuously measuring the mean of the distance from any point in the dataset to an arbitrarily placed cluster. The algorithm first defines a set of randomly positioned cluster centroids. It then methodically adjusts the positions of the clusters from their original random positions, in an operation whose goal is to minimize the sun of the distances between the clusters and all other data points assigned to them (Trevino, 2016) The “k” clusters that result from the operation can then interpreted as patterns that arise from the dataset. K-Means clustering is recommended for finding patterns in large datasets when there are no labeled data available (Trevino, 2016).

METHODS

In order to develop a machine learning algorithm that can create a geologic map that accurately represents the distribution of rocks on a field area, we had to first attempt a classification on a field area which would give the algorithms the best shot at working, a simple use case which

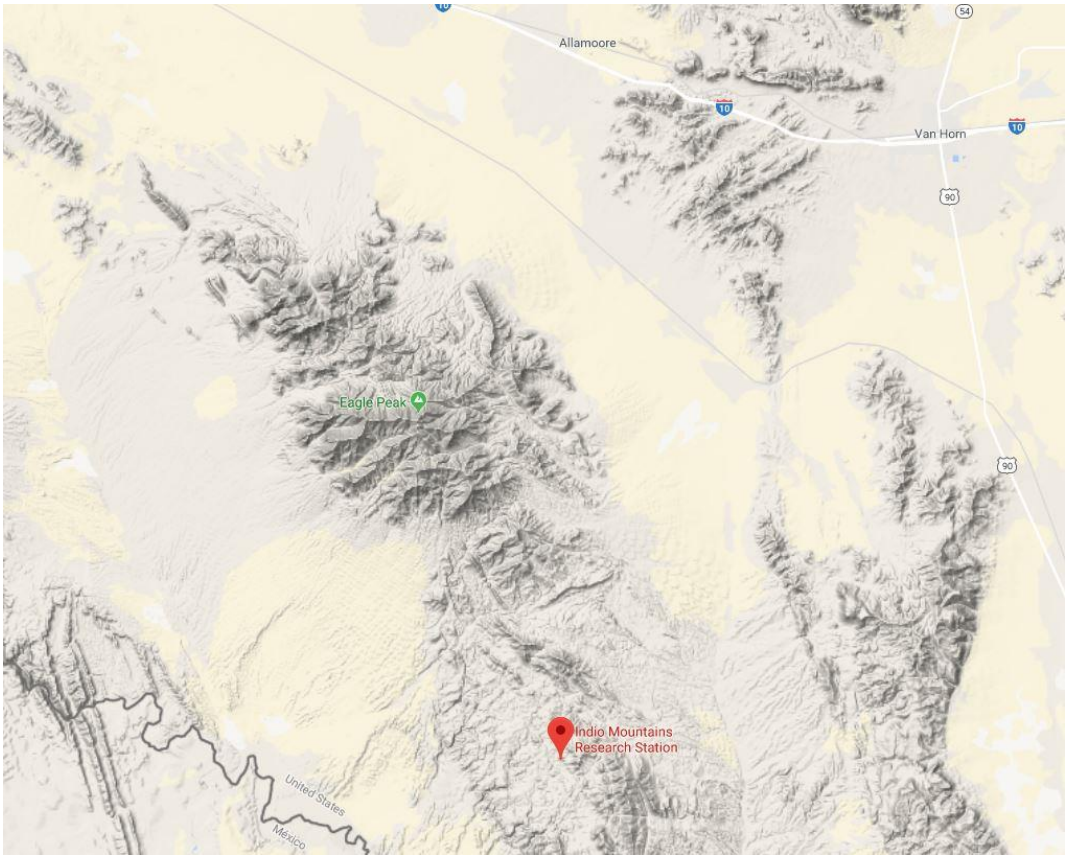

Figure 3. 1 Location of the field area – the Indio Mountains Research Station southwest of Van Horn, Texas – where we collected our data.

could determine whether feeding data into the algorithm could identify different rock units accurately. For this reason, we chose the Indio Mountains Research Station Area, 30 miles southwest of Van Horn, Texas. The location has geologic units that can easily be differentiated by

color only with the unaided eye. This way the rock units could be differentiated only by color and inexpensive sensors could be used to collect the data.

Data collection was performed with a 3DR Solo multirotor UAV Figure 3. 4 equipped with a GoPro Hero 4 camera to obtain natural color images of the field area. Images were obtained during autonomous flights at an altitude of about 150m above ground level. Autonomous flights were programmed using Mission Planner software (http://ardupilot.org/planner/)

3.1 Field Area

One of the requirements of the experiment were to have a small number of rock units exposed on the surface with very evident color distinctions. The Indio Mountains Research station, a property owned by the University of Texas at El Paso (UTEP) has several regions with a relatively simple distribution of rock units and the units have a very evident color difference. Of specific importance were the Lower Yucca Formation with a reddish coloration and the Bluff Mesa formation with a light gray coloration. There are also multiple geologic maps which were created by professional geologists and students alike, which would be used for ground-truthing the results.

3.1 Geologic Setting

The Indio Mountains Research Station is in Hudspeth County, Texas, approximately 20 miles southwest of Van Horn, Texas Figure 3. 1. Most of the property is owned by the university UTEP and a field station is located there. The Indio Mountains expose sedimentary rocks deposited during the Cretaceous period which have subsequently experienced Laramide compression and Tertiary extension and volcanism (Underwood, 1962). The Cretaceous sedimentary rocks – which include lacustrine, fluvial, and marine strata – were deposited in the Chihuahua trough, a northwest-southeast trending Mesozoic rift basin (Li, 2014). This stratigraphy is divided into six

formations. (from oldest to youngest): lower Yucca Formation, upper Yucca Formation, Bluff Mesa Formation, Finlay Formation, Benevides Formation, and Espy Formation (Underwood, 1962). The rocks record a constantly changing depositional environment in which both siliciclastic and carbonate rocks formed (Underwood 1962).

Figure 3. 2 The obvious color change between the lower Yucca Formation and the overlying, carbonate rich Bluff Mesa Formation. The contact between them is a thrust fault.

This study focuses on the Cretaceous Yucca and Bluff Mesa Formations. The Yucca Formation is the oldest of the two and comprises two members, the upper Yucca and the lower Yucca. The lower Yucca Formation is a conglomerate with a dark pink to reddish matrix, containing clasts from alluvial fans, braided streams, meandering streams, interbedded with the

conglomerate there are also discrete lacustrine deposits of lengths ranging from 40 – 20 meters that appear irregularly, occurring during localized flooding events that caused lacustrine depositional environments. (Fox, 2017; Underwood, 1962; Li, 2014). The distinct color of the lower Yucca formation makes it easy to identify in visible wavelength imagery.

The Bluff Mesa Formation is a gray to dark gray, fossiliferous and oolitic limestone interbedded with fine-grained quartz sandstone. The depositional environment for this unit was in normal marine conditions. The unit is easy to identify in outcrop due to the fact that it shows a large number of fossils, specifically foraminifera Orbitalina. (Li, 2014).

The contact between Yucca formation and the overlying Bluff Mesa formation is an abrupt fining upward transition from pebble conglomerate to a marine limestone with alternating bands of lacustrine silty deposits (Fox, 2017; Li, 2014). This contact is easy to identify in the field as a color change from the pink-reddish Yucca conglomerate to the tan/gray Bluff Mesa limestones.

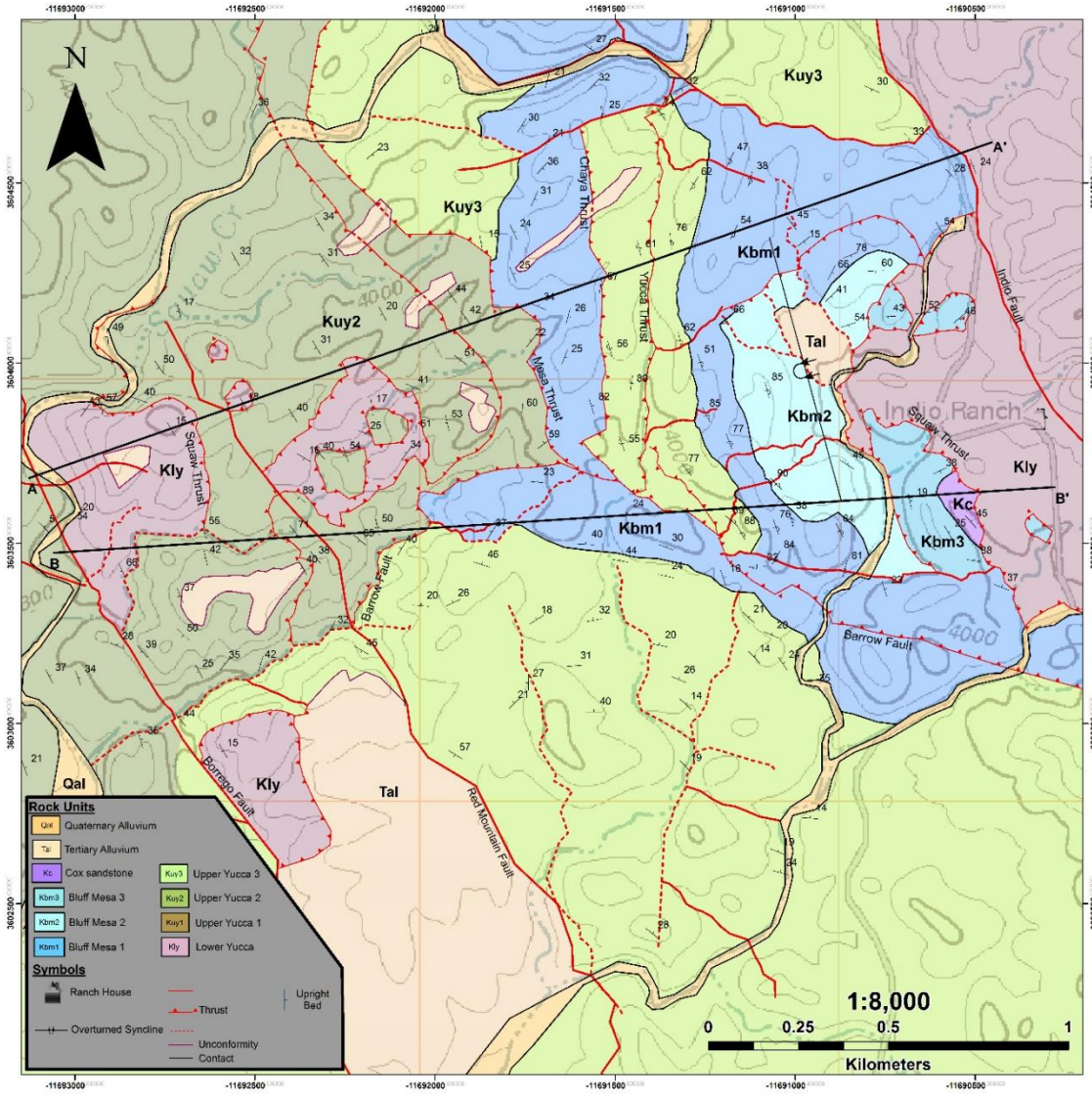

Figure 3. 3 Geologic Map of the Indio Mountains (Guerrero, 2018)

Because of this obvious color difference, this contact was chosen as the main target of the machine learning experiments described in this study.

3.3 Equipment Used

For the collection of data, we used a commercial drone platform the 3DR Solo Figure 3. 4, an excellent and stable platform that has fully autonomous flight capabilities and can be used with an open source software package called Mission Planner. Mission Planner was used to create autonomous mission plans.

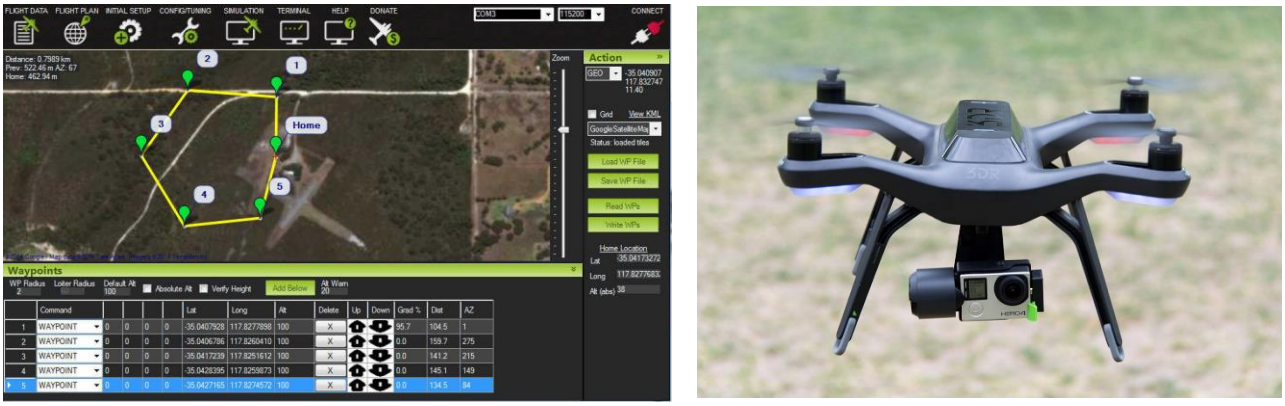

Figure 3. 4 Screen capture of the Mission Planner software used to plan autonomous UAV missions. (Right) The 3DR Solo quadcopter UAV used to acquire image data for this study.

The 3DR Solo was equipped with a GoPro Hero 4 Black high-definition camera which was used to obtain 1080-pixel resolution video. The pixel resolution of each image extracted from the footage recorder in the GoPro Hero 4 was approximately 7 cm/pixel. On some flights, the Solo was equipped with a Canon SD1400 IS digital camera modified to obtain near infrared images. The camera was modified by removing the infrared cut filter typically installed on consumer digital

cameras. Without this filter (also known as a "hot mirror"), the camera sensor is able to detect the full spectrum of light from the visible blue (~450 nm wavelength) to the near infrared (~800 nm wavelength). An additional modification added a blue color bandpass filter, this filter made the red channel sensitive to near infrared light, but the green and red light was blocked. The modified camera is capable of capturing near-infrared images along with blue light but was found to have significant limitations in its spectral resolution. Not enough detail is captured in the near-infrared to properly utilize the image spectra for classification purposes. For this reason, only visible spectrum data were utilized for the experiments.

3.4 Data Preprocessing and Conditioning

The data collection campaign produced 6 videos of the surface, these videos were then processed to extract images from the video every 5 seconds, this yielded 1,080 overlapping photographs. We then used an orthoimagery software called pix4D (https://www.pix4d.com/) to execute lens aberration corrections as well as the orthorectification. These images were then stitched together into an orthomosaic which then was used as the raw data for this project. The raw orthomosaic was then put through several pre-processing steps: First, we accentuated the color differences between rock units using histogram equalization contrast enhancement. **Error! Reference source not found.**6 shows the results of this enhancement. The contact between the reddish lower Yucca Formation conglomerate is clearly visible against the gray-green Bluff Mesa formation. To further increase the ability of the MLAs to distinguish the rock units and classify them correctly, we converted the images from their original red-green-blue (RGB) color space to the HSV (hue-saturation-value) color space. This color space transformation changes the representation of color from being a 3-channel pixel brightness in each of the red green and blue channels which has the

benefit that color is represented numerically by hue (Cheng et al., 2001). Machine vision algorithms use the color space transformation to detect colors that might be under different lighting conditions. Machine vision problems, such as road lane detection (Sqalli, 2016), use the hue to detect a color to more accurately than in in RGB color space irrespective of the time of day (Sqalli, 2016).

We then passed the HSV-transformed images through both a median filter and a Kuwahara filter. These two filters have the effect of blurring things like vegetation and roads on the image;

Figure 3. 5 Original RGB image (left) vs. contrast-enhanced RGB image (right) Contrast was enhanced using histogram equalization using a custom software built upon skimage.

this reduction of the noise helps the algorithm to better identify the patterns of rock units on the ground. An advantage of the median and Kuwahara filters is that they reduce noise and at the same time, preserve the contacts between rock units which might have been distorted by other filtering

operations. Previous work in machine learning recognition of salt in seismic data, has shown that the Kuwahara filter applied to seismic data significantly increases the accuracy of subsequent MLA recognition of salt in seismic sections (Qi et al., 2016). They observed that using the Kuwahara filter allowed MLAs to produce a more accurate geologic model. We employed a similar principle to the preprocessing of our images.

Figure 3. 6 Output after median filter and Kuwahara filter operations, which together remove vegetation while preserving the edges of each rock unit on the ground. The left image is the original, unfiltered image, and the left image is the result of the median and the Kuwahara Filter.

All the pixels on the image were then normalized, this operation equalizes the "importance" of the numeric magnitude of individual pixels in the image. This means that higher magnitudes of pixels did not have *an overpowering* impact on the fitting of the MLA model. This is standard procedure for machine vision problems (Dietterich, 1995) because it ensures that all observations contribute to the final training of the model and that large values do not cause overfitting.

The final pre-processing step we applied, which is standard in machine vision problems (although of less importance to certain algorithms), is shuffling the dataset (Brown, 1999). This operation minimizes the risk of overfitting a MLA because images contain regions and not necessarily randomized data. This risk occurs because as will be explained in the following section,

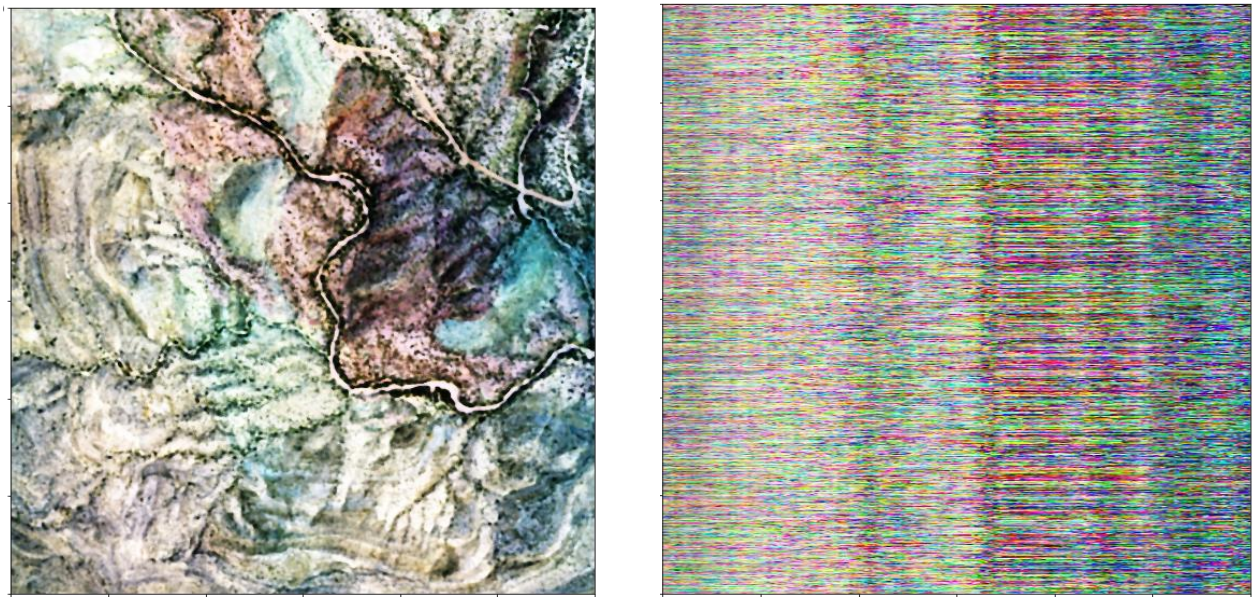

Figure 3. 7 Result of shuffling the original RGB image dataset. Note that the patterns visible on the left are completely destroyed in the resulting image on the right.

the dataset will be split into a training and a testing dataset; depending on where the split occurs, it might be possible that, for example, the training split will contain a majority of a certain label, and conversely the test split can contain a minimal amount of labels in the aforementioned training split. Not randomizing in this scenario will lead to the algorithm being overconfident and misidentifying data points because of it was overfitted to those points that are in the majority of the dataset. The order of pixels in the image matrix was shuffled by taking one pixel and moving

it to a random location in a resulting image. The output is a random distribution that destroys the spatial patterns in the scene and can thus be split safely Figure 3. 7.

Surprisingly, even though the shuffled dataset makes no sense to the human eye and it unclear how to deduce any pattern from the image, the MLAs translate the data points and values into what amounts to a different dimension called feature space. In the case of the image it contained the 4 channels of RGB and H and in feature space the MLAs are able to make sense of the data.

3.5 Machine Learning Algorithm Training

Once the preprocessing workflow was completed, the supervised MLAs could be trained. Note that the unsupervised MLAs do not require training. Two approaches were used for supervised MLA training and we tested their comparative effectiveness at classifying the lower Yucca and Bluff Mesa Formations.

The first training approach was to take an individual stack of pixel values (RGBH) and use the corresponding label to train the algorithm to recognize each pixel stack. This approach has the advantage of higher level of detail because each pixel location is observed with more detail in comparison to analyzing an area of pixels. A disadvantage of this approach is that the result came out extremely noisy and in order to generate something that looked more like a geologic map, other processes had to be done on the results, we will look at this in more detail later. We believe that the introduction of noise issue is mitigated by the application of the median and Kuwahara filters in the preprocessing step, where the filters blur out vegetation and other high frequency variations of pixels (Pinheiro et al., 2015).

The second training approach was to consider a square pixel neighborhood stack of various sizes, rather than only a single pixel stack. The pixel neighborhood stacks are then labeled, and the algorithm learns to recognize a "patch" instead of a single pixel stack, this is like the process of detecting a handwritten number; the full number image is observed by the MLA not, each individual pixel. This method can reduce the amount of salt and pepper noise in the output map as will be shown in Chapter 4. The main reason for trying the pixel neighborhood stack was to train the algorithm with a larger sample of pixel values. We believe that this allows for more accurate labeling of rock units on the ground even in areas obscured by mild vegetation.

The most important requirement for training the supervised MLAs is labeled data. The process of labeling proved to be more challenging than the actual training and application of the supervised MLAs. Because the Indio Mountains field area has never been explored specifically with supervised MLAs there was no available training data, so those datasets had to be generated. To this end, we built a pixel-wise and neighborhood classifier tool in Python from scratch. We built a simple interface that displays the preprocessed image to be analyzed an allows a user to manually click on pixels in the image to label them by deciding whether the pixel is red or green. This was done both for the pixel wise and neighborhood approaches. For the neighborhood labeling process, the user clicks a pixel that belongs to a category and the program records the pixel values, position, and label of a pixel block of size n. The training data were then stored and utilized to train the supervised MLAs to recognize the rock units, the training operation. There exist multiple geologic maps that have been generated by human geologists; these maps could be used to create labels for a region, but in this project, we decided to create the labels by very carefully zooming into a subset of the whole region and clicking the appropriate button to label the features.

The training operation is quite simple, the dataset needs to be split into two subsets. The first subset is the training data set and the second subset is the testing data set. This is common practice in MLA development. The training split is a subset of the original dataset which contains most of the data points, this split is used to train the actual algorithm. The actual training of the algorithm is very straightforward and only requires the algorithm to be fed the dataset and the rest is waiting for it to finish. The test split is essentially a way of executing some ground truthing, to verify that the algorithm can accurately identify a feature that we know is labeled correctly (as it comes from the originally labeled training dataset). This process will be discussed in more detail in chapter 4.

RESULTS AND DISCUSSION

4.1. Pixelwise Analysis and Mapping Using Unsupervised MLAs

The first experiment was to classify the pre-processed UAV orthoimagery with the K-Means clustering MLA. This algorithm produces an initial set of randomly generated classes into which every individual pixel or neighborhood (depending on the pre-processing scheme used) is then assigned membership. The locations of these classes within the feature space of the image, continuously adjusts in an iterative manner until an optimum placement is reached, by minimizing the mean distance from data points to the class (centroid). We experimented with various numbers of initial classes of clusters and noticed that by increasing the number of clusters generated from the shuffled dataset, the algorithm produced a more detailed, albeit not necessarily accurate, segmentation of the potential rocks on the ground. This was not necessarily a good thing because, the algorithm tended to define more rock unit classes than what we knew actually were there, i.e. two (the Yucca and Bluff Mesa Formations). Even though it might be possible for the algorithm to have produced an even better segmentation of the units present on the ground, after a qualitative analysis of the results, the spectral resolution of the instruments used for this study could not possibly provide the basis for this; it is possible that with better instruments the algorithm will produce a better segmentation of the geological units on the ground. Another issue was that the more clusters were extracted by the algorithm, the more post-processing work needed to be done to identify correct classifications and merge classes that are equivalent, and thus minimize the deviation of the generated geologic map to the one produced by a professional human geologist. This post-processing is time consuming and does not necessarily result in a more accurate classification than the supervised algorithms and certainly not more accurate than a human executing the classification.

Figure 4. 1 shows the results after setting the initial conditions of a maximum of 3 clusters possible in the output. The algorithm recognized both the Yucca and the Bluff Mesas Formations without any explicit input from the user on how to segment the dataset. The magenta pixels in the

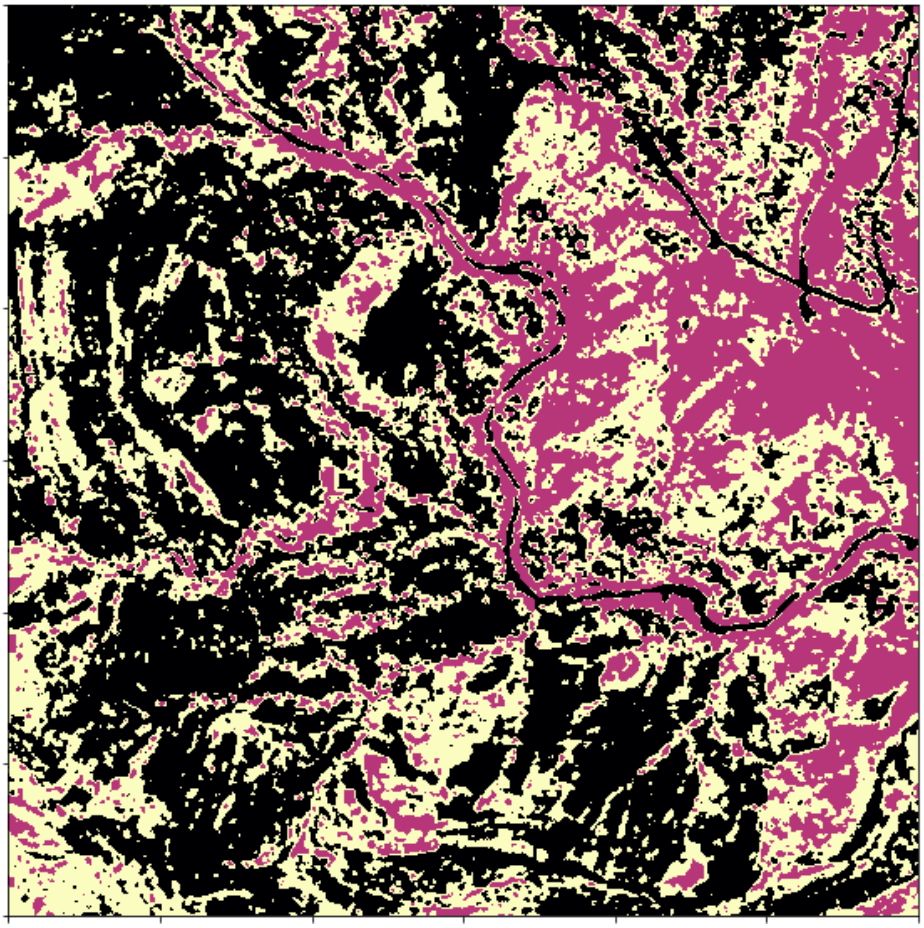

Figure 4. 1 Output of the K-Means Clustering algorithm with a maximum of 3 clusters. The algorithm identified Bluff Mesa formation in black, and Lower Yucca Formation in Pink, there is another color present on the scene, which is highly unlikely to be another rock unit.

eastern half of the image were classified as lower Yucca Formation and the black pixels in the western half of the image were classified as Bluff Mesa Formation. The yellowish pixels belong to a class that could correspond to a variation of the Bluff Mesa Formation mapped by (Guerrero,

2018). This unit could be Tertiary Alluvium (Tal) and may have been identified as a distinct class by the algorithm because of detectable variations in color, linear features detectable on the image, or vegetation affecting the algorithm. From the results is unclear if someone without reference to a geologic map could have identified it as a separate rock unit. The main reason that the algorithm detected more patterns is because the algorithm was forced to identify three clusters.

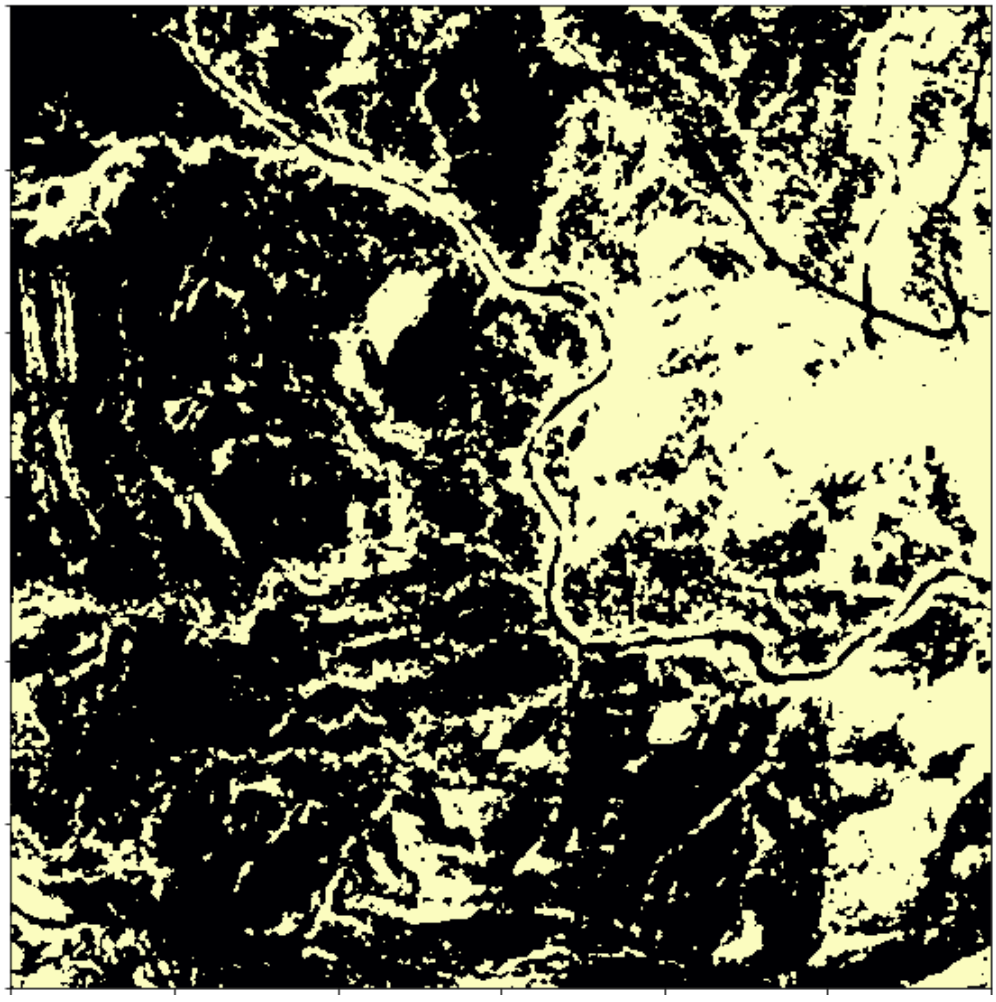

Figure 4. 2 The output of the K-Means clustering algorithm with only two clusters selected. The yellow color was interpreted as the lower Yucca Formation in the eastern and the black color was interpreted as the Bluff Mesa Formation.

Figure 4. 2 shows the same scene subset as Figure 4. 1. The only difference is that the algorithm in this case was forced to only recognize 2 clusters. The experiment sought to generate as close an approximation as a regular geologist produced geologic map as possible, and since most maps show a maximum of 2 rock units (Guerrero, 2018) on the area surveyed by the UAV, the two-cluster output should be closer to the distribution of rocks on the ground. The segmentation

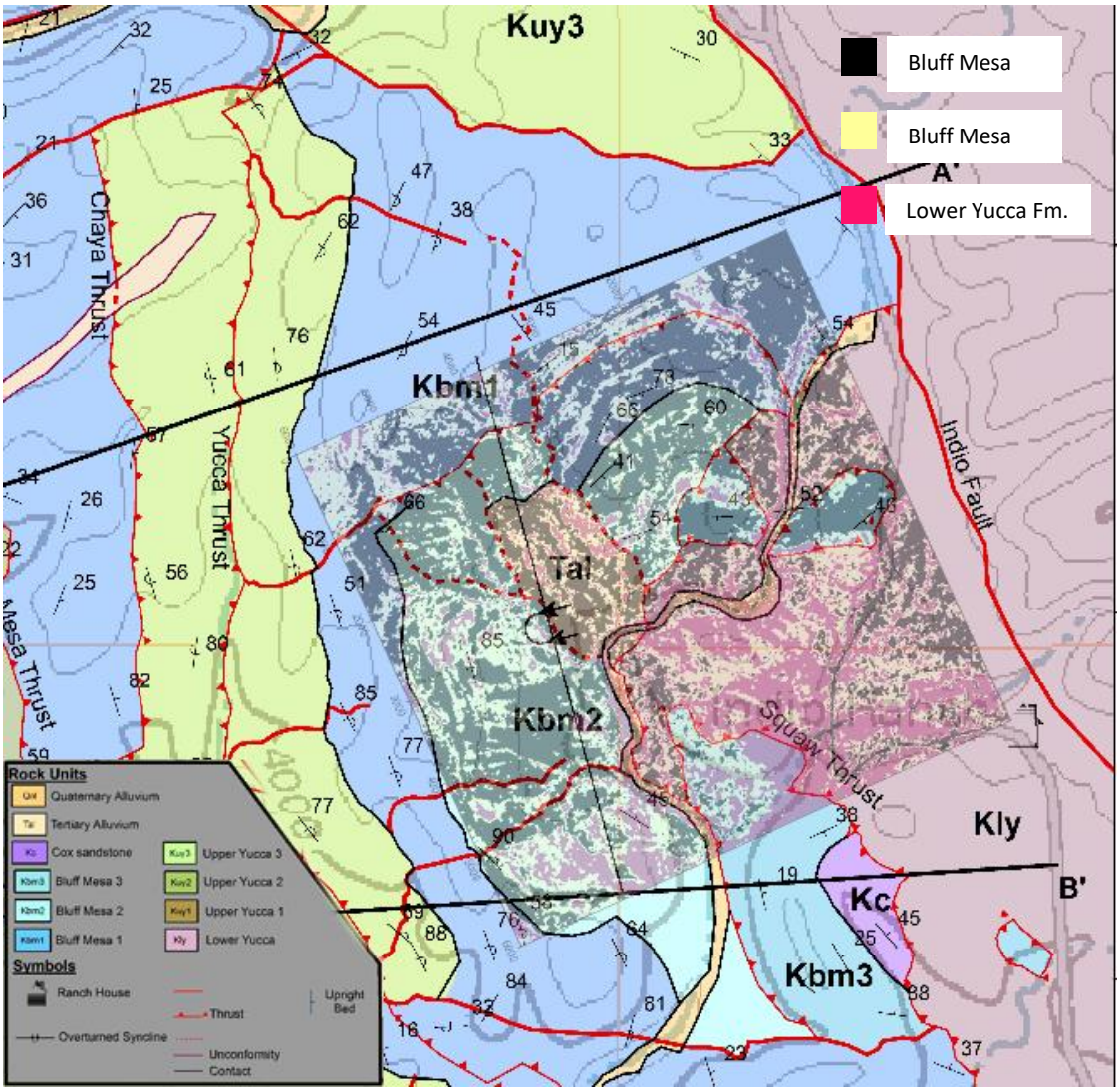

Figure 4. 3 Geologic map of the Indio Ranch area (Guerrero, 2018), with the K-Means 3 clustering result as an overlay.

between Bluff Mesa in black and the Lower Yucca Formation in Yellow was assessed qualitatively to be more accurate in comparison to a geologic map of the area (Guerrero, 2018).

4.2 Pixelwise Classification and Mapping Using Supervised MLAs

Although unsupervised classification algorithms can be very useful in quickly determining a broad picture of the potential distribution of rocks on the ground, supervised classification algorithms are far superior at image recognition (Guerra, et al., 2010). We employed various supervised algorithms and the same training data used for the unsupervised MLAs was used for all supervised MLA experiments.

The first step in the implementation of supervised MLAs was to attempt the classification of the geology on the ground by analyzing each pixel of the image dataset individually. Each UAV image has a resolution of approximately 25 cm/pixel, which is a good resolution for observing objects, but for the purposes of this study, spatial resolution is not as important as the radiometric resolution of the imaging sensor. We are detecting spectral differences between rock units, so the most important aspect is the camera's ability to capture details about the colors and hues of the rocks on the surface.

The data that were used to train the supervised classification algorithms were generated by creating what are called "one-hot" arrays. One-hot arrays are multidimensional vectors which use a binary labeling scheme. A label, whose value corresponds to the presence of a particular rock unit is added to each pixel location in the image. The label is a 1 or a 0, where 1 represents the presence of a specific class and 0 represents the absence of that class. A combination of one-hot arrays is then stacked and converted into a flattened list by using a custom software tool. These stacks are then used as input by the MLA and the algorithm uses this input to generate a trained machine learning model that can predict a classification from any given pixel brightness value of

the processed image dataset. The high misclassification rates produced many areas of noise-like patterns, and these maps are essentially useless, some regions of Lower Yucca represented by the white colors in Figure 4. 4 can be differentiated from the Bluff Mesa Formation represented in

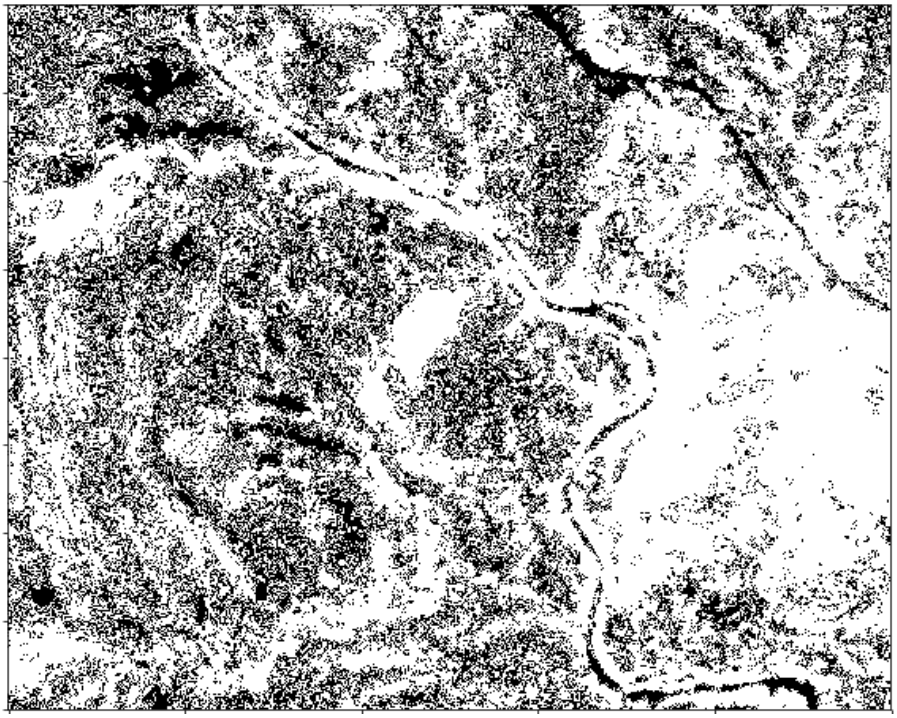

Figure 4. 4 The raw output of the k-NN algorithm classification. Notice the high amount of noise and low readability of the boundaries of the rock units. In this scene the white pixels were identified as the Lower Yucca Formation, and the black pixels were classified as Bluff Mesa Formation

black color, but the level of detail is greatly reduced. In order to make this map more useful, we had to remove the noise somehow. We reduced the resulting "salt and pepper" patterns in the results by applying a combination of morphological operations: binary dilation, and median filtering on the binary result. The result is a distribution of rocks that matches the geologic map used for qualitative assessment of prediction accuracy (Guerrero, 2018).

The key takeaway from running the classification K Nearest Neighbor algorithm is that the algorithm was able to detect the lower Yucca Formation and the Bluff Mesa Formation using only the training data rather than using a rule-based approach where a certain pixel value acts as a threshold to output classifications; the raw results had a lot of noise in them and filtering

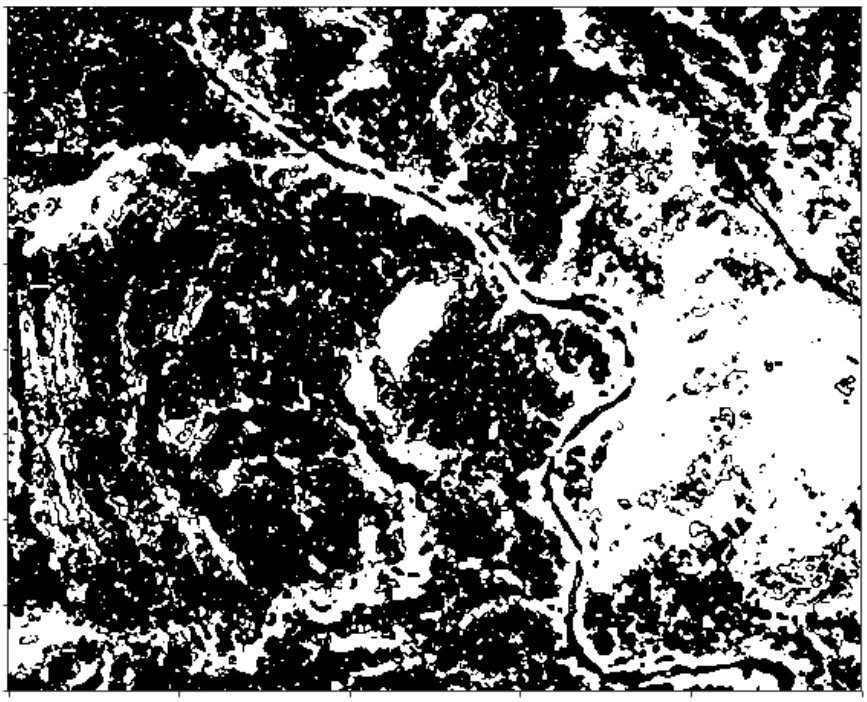

Figure 4. 5 The result of the multiple filtering operations from the raw output of the K Nearest Neighbor Pixelwise Classification technique. The "salt and pepper" patterns are now greatly reduced and a clearer distinction between the Bluff Mesa Formation(black) and the Lower Yucca Formation (white) can be observed.

operations had to be executed to make a better approximation of the rock contacts. We tested the accuracy of the algorithm by using the test split of the dataset. The precision report for the pixelwise classification operation is shown in Table 4. 1. The percentage of error for classification of known labels that the algorithm produced is in the accuracy column.

Table 4. 1 Precision report for pixelwise classification using K Nearest Neighbor Algorithm. The label prediction accuracy represents the percentage of times that the algorithm successfully predicted a known label from the test split of the dataset.

Rock Unit Name	Label prediction accuracy
Bluff Mesa	69%
Lower Yucca	48%
Total Combined Accuracy	61%

4.3 Neighborhood Analysis and Mapping Using Supervised MLAs

Pixelwise classification detected the differences between rock units, but it had its shortcomings such as a lot of false positive identifications. One of the contributing factors to misclassification is vegetation. The color difference between vegetation and underlying rock caused some mislabeling. This was especially the case with the Bluff Mesa Formation, which looks visibly greenish and was often confused with vegetation and vice versa by the algorithm. This was a widespread issue in the classification, and, although we tried to minimize the effects of vegetation by applying the Median and Kuwahara filters, the vegetation problem influenced the classification of pixels. Although the presence of vegetation could be exploited to detect rock units associated with vegetation types (Cuyler, 1931), that application would require substantial adjustments to the processing workflow.

To overcome the shortcomings of the pixelwise classification, we experimented with another method to mitigate the effect of vegetation as discussed in the background section. A similar approach is used in other machine vision applications such as in the task of recognizing handwritten digits (scikit-learn developers, 2018), human faces (scikit-learn developers, 2018), and decide whether an autonomous car should drive left or right (Chaudhari et al., 2018).

The approach required collection of large numbers of pixel neighborhoods, 670 of them to be precise. The size of the neighborhoods was set to 10 x 10 pixels (0.7 m per side and an area of 0.49 m^2 per neighborhood). Where vegetation was present, the pixel neighborhoods include both

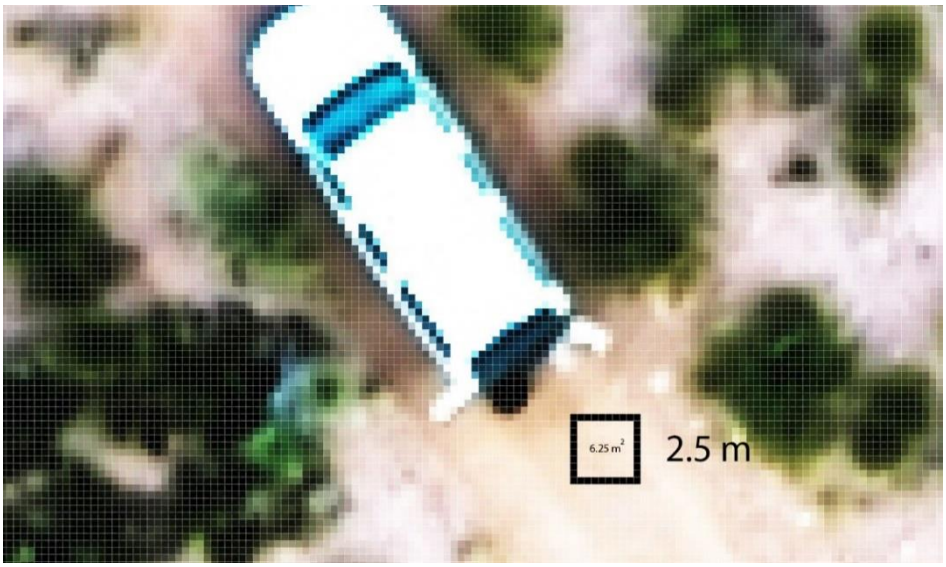

Figure 4. 6Area represented by the neighborhood. The square is a graphical representation of the collection of pixels. 10 pixels wide. This translates to each side of the neighborhood being 0.5 m per neighborhood.

vegetation and rock. This meant that the algorithm was trained taking into account the vicinity of the plant, which contains information about the rock unit the plant is growing on.

This approach yielded a small increase accuracy of the classification but was much more computationally expensive in comparison to the same algorithm using pixelwise classification. The neighborhood classification results in Figure 4. 7(From left to right) The results of the SVM classification, the K-Nearest Neighbor classification (post-filtering), and the color enhanced image. The first image shows the Lower Yucca Formation in black obtained via the SVM algorithm, the middle image is the K-Nearest Neighbor algorithm result showing the Lower Yucca

Formation in white., for example, took 31,526 seconds (8 hours) to produce compared to 1,517 seconds (25 minutes) to produce the pixelwise classification result. It is important to keep in mind that these processing times are also a function of the custom software used and the algorithms not being optimized and not being designed to exploit parallel processing.

Due to the small size of the training dataset, the results contain multiple false positives. Figure 4. 7(From left to right) The results of the SVM classification, the K-Nearest Neighbor classification (post-filtering), and the color enhanced image. The first image shows the Lower Yucca Formation in black obtained via the SVM algorithm, the middle image is the K-Nearest Neighbor algorithm result showing the Lower Yucca Formation in white. shows the results of the SVM algorithm trained with a neighborhood of pixels in comparison to the SVM algorithm trained with only individual pixels. The first map from the left shows the result of the SVM neighborhood classification, where black denotes the lower Yucca Formation. The second map from the left is the result of the SVM algorithm trained with individual pixels, where white denotes the lower Yucca Formation. The SVM algorithm using the neighborhood classification produced what qualitatively can be interpreted to be a more complete identification of the lower Yucca Formation in the east portion of the map, with fewer gaps and less influence from vegetation. Some pixels were identified as Bluff Mesa Formation even though they clearly look like upper Yucca Formation in the original color image. One explanation for the misclassification could be that in the eastern portion of the image, on the location of the Lower Yucca Formation which appears red, there are areas with green pigmentation within the rock unit. We believe that this green pigment in combination with the Lower Yucca formation color caused those misclassifications.

We ran an accuracy report with the test split of the dataset as discussed in the methods section. The test showed that the neighborhood-trained SVM algorithm had a 20% greater accuracy compared to the pixelwise-trained SVM algorithm. The maps show clear discrimination

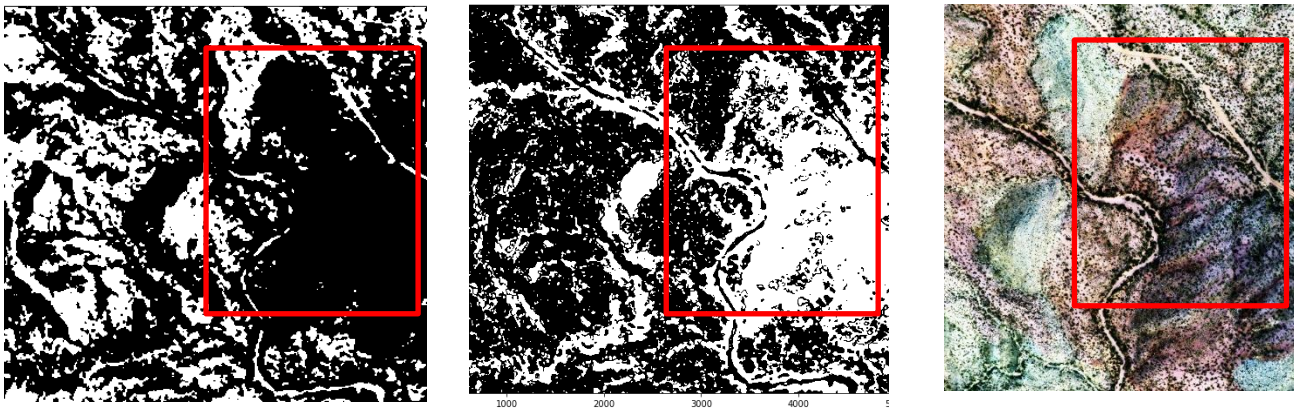

Figure 4. 7(From left to right) The results of the SVM classification, the K-Nearest Neighbor classification (post-filtering), and the color enhanced image. The first image shows the Lower Yucca Formation in black obtained via the SVM algorithm, the middle image is the K-Nearest Neighbor algorithm result showing the Lower Yucca Formation in white.

of the lower Yucca Formation from the Bluff Mesa Formation in the east half of the image, whereas the classification introduced a lot of false positives in the other western half of the image. This could be due to the hue in the left half of the image is perceivably lighter and getting interpreted as closer to green and hence to the Bluff Mesa Formation.

During the process of training the SVM algorithm the dataset must be split and shuffled. One of the outputs of splitting is a data set used for training and another for testing. The testing data points can then be used to ground truth and quantify the predictive abilities of the algorithm. Table 4. 2 shows the precision report for the SVM classification using the neighborhood training set.

Table 4. 2 Precision report for neighborhood classification using the SVM algorithm.

Rock Unit Name	Label prediction accuracy
Bluff Mesa	77%
Lower Yucca	65%
Total Combined Accuracy	72%

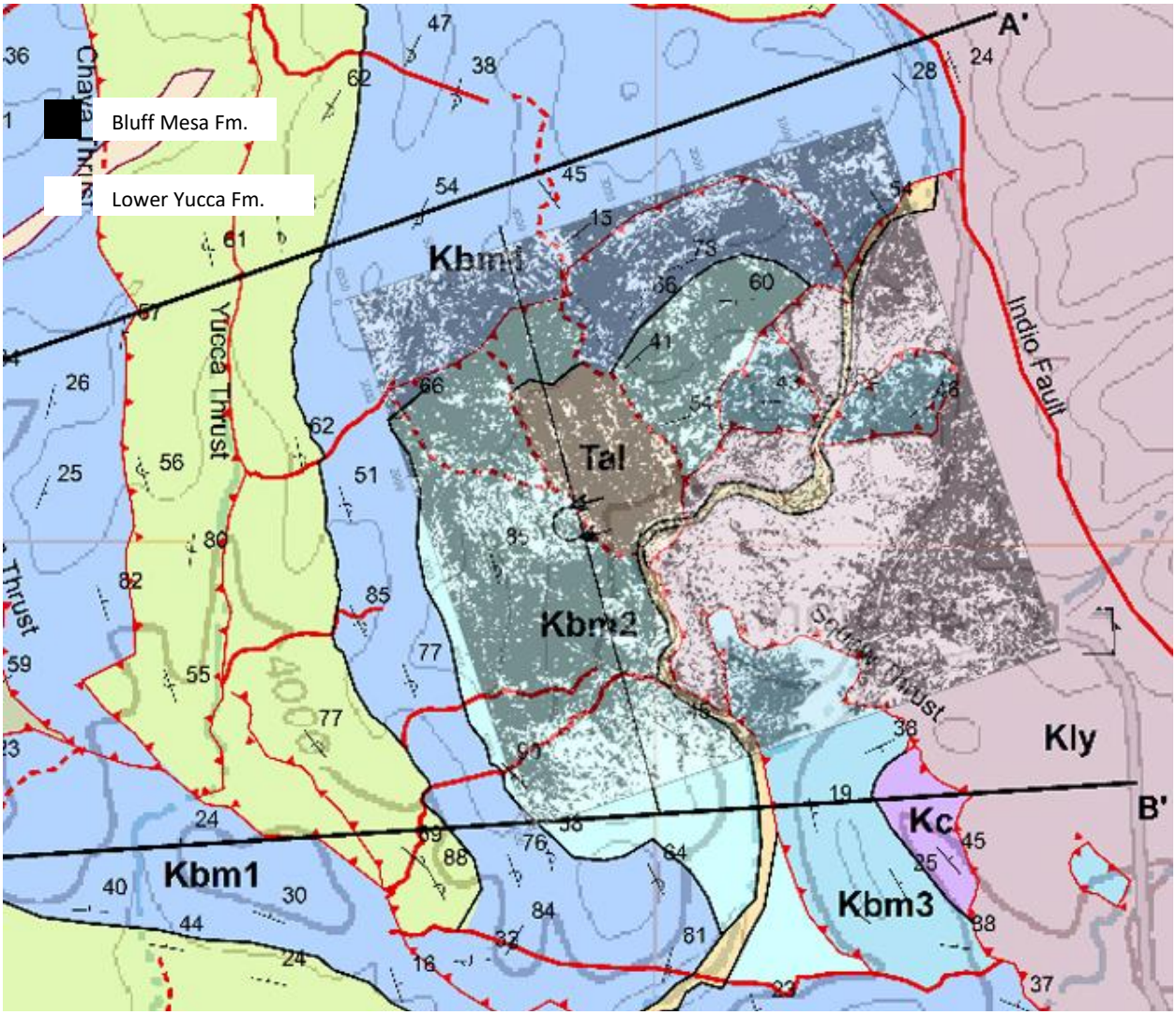

Figure 4. 8 Geologic map of the Indio Ranch area (Guerrero, 2018), with the SVM algorithm trained with pixel blocks result as an overlay. The clustering result shows the Bluff Mesa formation in black and the lower Yucca Formation in white. The lower Yucca Formation was identified with some errors, and the Bluff Mesa Formation was better identified, but with some misclassified points.

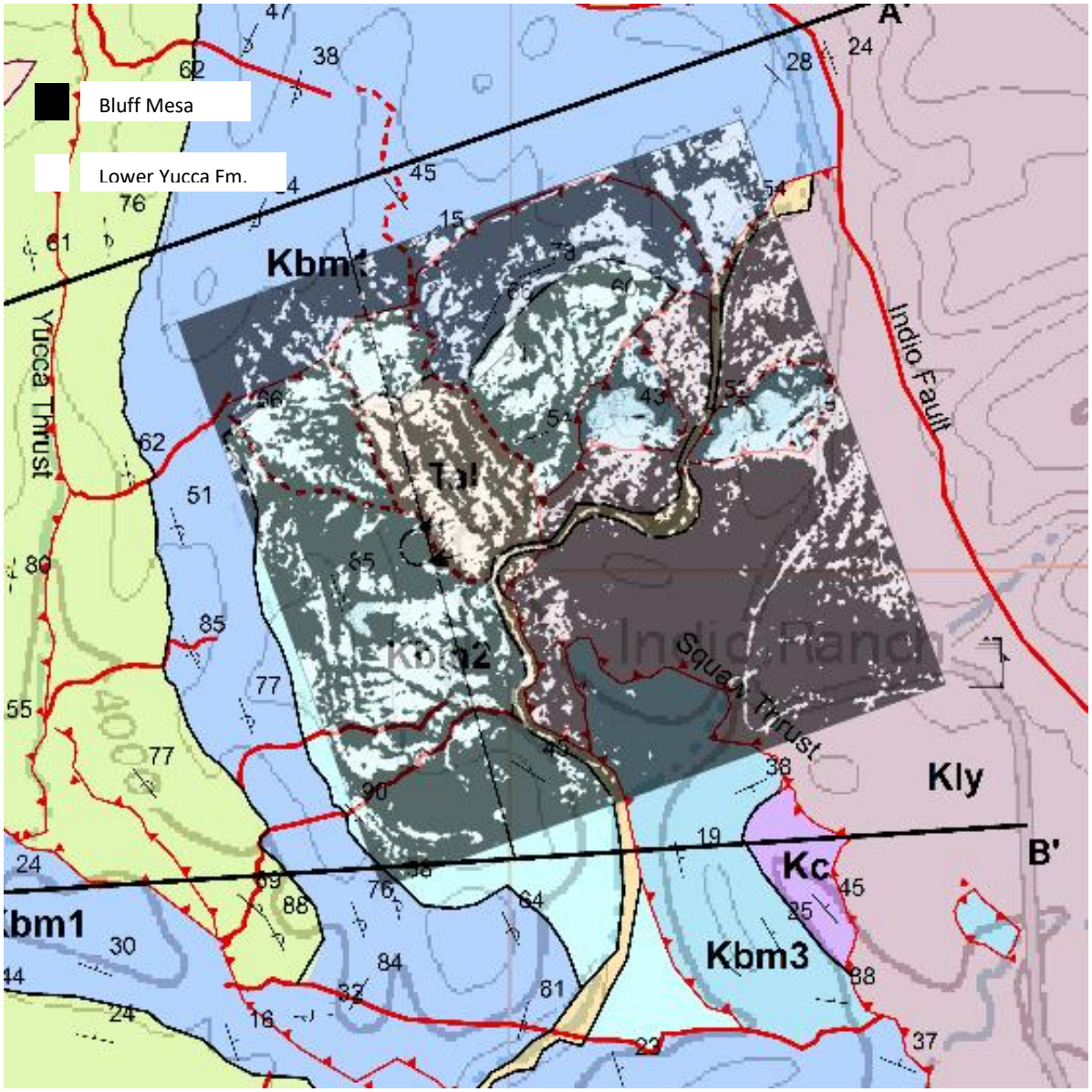

Figure 4. 9 Geologic map of the Indio Ranch area (Guerrero, 2018), with the SVM algorithm using pixelwise classification result as an overlay. The algorithm detected a large portion of the lower Yucca Formation and partially recognized the Bluff Mesa Formation.

4.4 Pixel Neighborhood Analysis and Mapping Using Convolutional Neural Networks

We tested the capabilities of the CNN algorithm of predicting geology from the images. For this we employed Google's TensorFlow library, which is an open source symbolic math framework used to create convolutional neural networks. We used the same neighbors as the SVM algorithm, modifying the parameters of the algorithm to fit the size of the 10x10 pixel neighbor blocks. Due to the small number of training data points, the algorithm only took 45 seconds to train with 200 epochs of training. The output image subset took 31,759 s (8 hours) to be generated. The reason why it took so long is because the algorithm does the classification one pixel at a time. In principle, this could be improved by taking advantage of parallel processing. Using the same testing method as with the previous supervised algorithms, we obtained an 82.3% accuracy for the test dataset. Note that this does not mean that the resulting map is 82.3% accurate. In fact, the resulting accuracy of prediction of the known data points is very similar to that of the SVM algorithm . This similarity was also observed in work by Petropoulos et al. (2012) who found that SVM only slightly outperformed CNN. We believe that CNN would eventually outperform all other algorithms with a large enough training dataset. Even with limited training dataset, the CNN algorithm learned to recognize the differences between Yucca Formation pixels and Bluff Mesa pixels on its own using the training label provided.

Figure 4. 10 Results of the Convolutional Neural Network algorithm. It detects the boundaries of rock units, just as accurately as the SVM algorithm. The black color is the Lower Yucca Formation and the white color is the Bluff Mesa Formation.

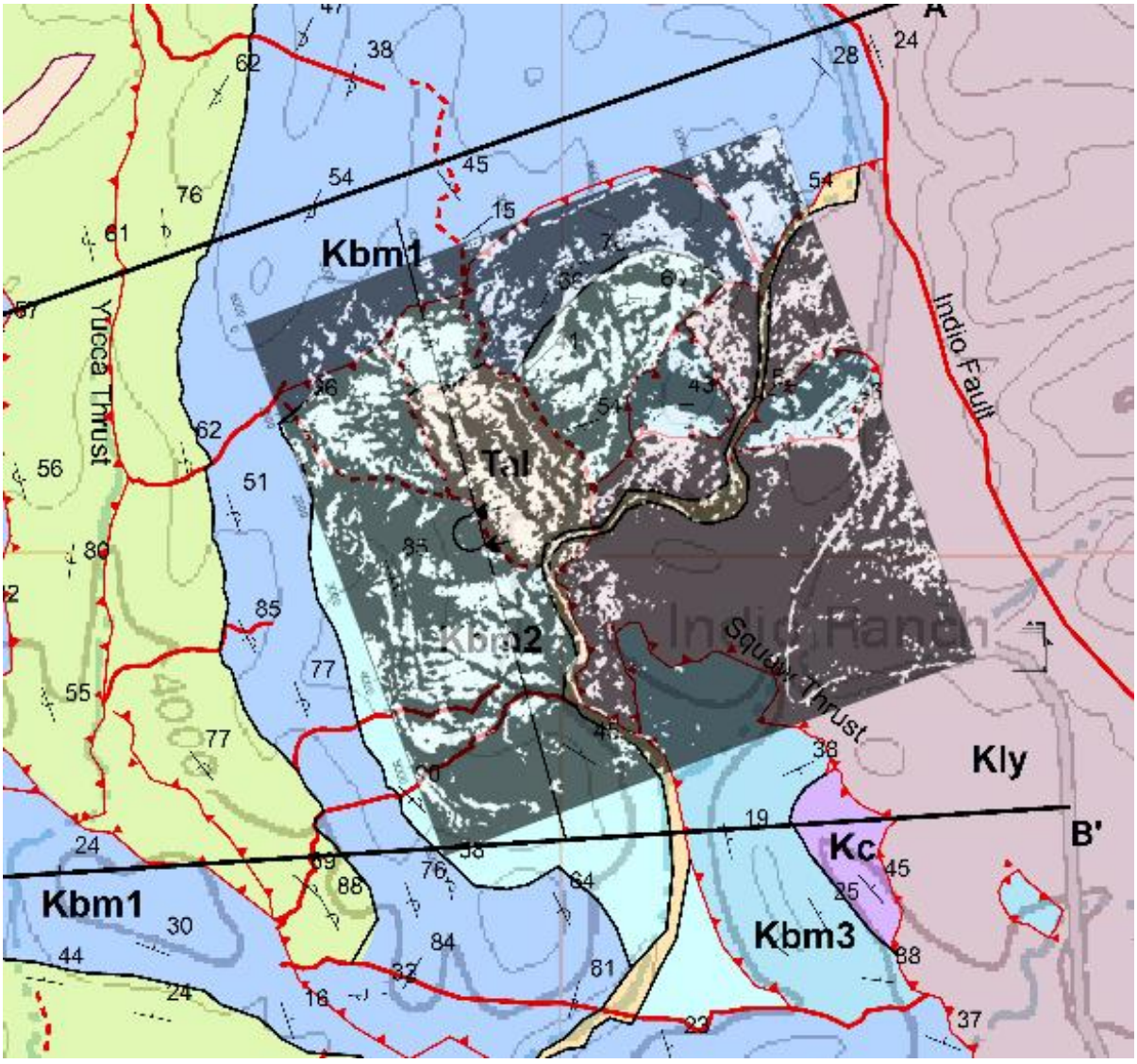

Figure 4. 11 Geologic map of the Indio Ranch area (Guerrero, 2018), with the Convolution Neural Network result as an overlay.

CONCLUSIONS

The machine learning algorithms we tested were able to recognize and distinguish between the Yucca Formation and the Bluff Mesa Formation by using a trained dataset and minimal input from the user. All of the classifications yielded false positives, where the predicted rock unit was not correct. This could mostly be due to the size of the training data set. If the amount of data points in the training set is increased in both samples as well as other features, the algorithm will increase its predictive abilities. We believe that vegetation played a role in the misclassification of some regions where a green hue dominated the scene. This could potentially be reduced using near-infrared imagery. Near-infrared measurements can be used to compute the Normalized Difference Vegetation Index (NDVI), a spectral index used to detect the health and location of plants in comparison to other land cover (Pettorelli, 2013). Using the NDVI data points, we could label pixels that fall within a certain threshold as plant material. The NDVI dataset and labels could be inserted into our training set as a way to eliminate vegetation pixels from consideration as rock units. We propose doing this as a next step in this research.

The number of features is crucial because although two distinct rock units can be distinguished simply by color, there are many other observations that should be included. Color can be an excellent distinguishing feature, but it is not always the clearest way of distinguishing rock units, as is the case with very similar looking rock units. Color, in combination with other features like infrared reflectance, gravity, magnetics, etc. can be gathered into an excellent training data set, and with those extra features the algorithms will increase their ability to recognize differences between rock units.

One outcome of this project is a trained model of the Indio Mountain geology; this algorithm can be downloaded and used by anyone and to achieve results such as the ones described in this paper they would not require any retraining. Any other geologist that would like to use these trained algorithms could get them from a server and immediately use the classification abilities with the appropriate tools. This concept of training and storing the machine learning models can be converted into a vast library of trained algorithms, trained in multiple geologies; these models can be retrieved and used by people around the world. As the algorithms are used, and their classification abilities are refined with new training data, they will become better at the classification task. This is similar to the way that Google produce vast amounts of data for their facial recognition algorithms. They provide free unlimited image storage to the user and in return Google gets data they could use to train their algorithms (Luckerson, 2017).

Regarding the algorithms we trained in this project, we can say that the algorithms did not provide a completely satisfactory geologic map, but it is a very encouraging starting point. The maps showed correct locations of several rock distributions on the ground but missed a lot of locations where it did not classify the units correctly. The algorithms show clear potential, and the inaccuracies they suffer are mainly a factor of the quality and quantity of training data available. In this study we decided to run MLAs with very basic RGB image data of the sort that would be available to a regular consumer.

The sensors used to collect the data were consumer-grade cameras with an 8-bit radiometric resolution. Recently 10-bit radiometric resolution cameras have become available to the consumer which have a higher radiometric resolution than any previous consumer-grade camera. A camera like this would make a difference in the performance of machine learning algorithms applied to image classification for geologic mapping purposes. In the future we would also like to increase

the number of features used to train the algorithm. Features such as NDVI for vegetation, hyperspectral images, textural features obtained by Lidar or Radar sensors and gravity and magnetic geophysical measurements. These may be used as features that can help the algorithm to better identify the rocks on the ground.

6. BILBIOGRAPHY

Ahmad, L., Shah, M. T., & Khan, S. D. (2016). Reflectance spectroscopy and remote sensing data for ... *Earth Science Informatics, 9*(1), 113-121. Retrieved 9 14, 2017, from https://link.springer.com/article/10.1007/s12145-015-0239-x

Alpaydin, E. (2010). *Introduction to Machine Learning.* Cambridge: The MIT Press.

Altman, N. (1992). An introduction to kernel and nearest-neighbor nonparametric regression. *The American Statistician,* 175-185.

Altman, N. S. (1992). An introduction to kernel and nearest-neighbor nonparametric regression. *The American Statistician,* 175-185.

Anthony, E. Y. (1992). Compositional diversity in late Cenozoic mafic lavas in the Rio Grande rift and Basin and Range province, southern New Mexico. *Geological Society of America Bulletin*, 973-979.

Berni, J. A., & Zarco-Tejada, P. J. (2009). REMOTE SENSING OF VEGETATION FROM UAV PLATFORMS USING. *Int. Arch. Photogramm. Remote Sens. Spatial Inform. Sci*.

Biedelman, I. (1985, October). Human image understanding: Recent research and a theory. *Computer Vision, Graphics, and Image Processing, 32*(1), 29-73.

Bolton, T. (1989). *Geological Maps: Their Solution and Interpretation.* Cambridge: Cambridge University Press.

Borengasser, M., Hungate, W. S., & Watkins, R. (2008). *Hyperspectral Remote Sensing: Principles and Applications.* Boca Raton, FL: CRC Press.

Brown, M. (1999, 11 05). *Support Vector Machines*. Retrieved 2018, from SVMs for gene expression data : https://compbio.soe.ucsc.edu/genex/genexTR2html/node3.html

Burl, M. (1998). Learning to recognize volcanoes on Venus. *Machine Learning*, 165-194.

Carceroni, R. L., Kumar, A., & Daniilidis, K. (2006). *Structure from Motion with Known Camera Positions*. Retrieved 9 17, 2017, from http://cis.upenn.edu/~kostas/mypub.dir/carceroni06cvpr.pdf

Chaudhari, R., Dubey, S., Kathale, J., & Rao, R. (2018). Autonomous Driving Car Using Convolutional Neural Networks. *In 2018 Second International Conference on Inventive Communication and Computational Technologies*, 936-940.

Cheng, H. D., Jiang, X. H., Sun, Y., & Wang, J. (2001). Color image segmentation: advances and prospects. *Pattern Recognition*, 2259-2281.

Christensen, P. R. (1993). Thermal infrared emission spectroscopy of natural surfaces: Application to desert varnish coatings on rocks. *Journal of Geophysical Research: Solid Earth*, 19819-19834.

Coomans, D., & Massart, D. (1982). Alternative k-nearest neighbour rules in supervised pattern recognition : Part 1. k-Nearest neighbour classification by using alternative voting rules. *Analytica Chimica Acta*, 15-27.

Cornelisse, D. (2018, Apr 24). *An intuitive guide to Convolutional Neural Networks.* Retrieved from Medium: https://medium.freecodecamp.org/an-intuitive-guide-to-convolutional-neural-networks-260c2de0a050

Coursera. (2017, January 3). *Coursera Blog*. Retrieved October 17, 2017, from Coursera Blog: https://blog.coursera.org/popular-courses-2016/

Cover, T. &. (1967). Nearest neighbor pattern classification. *IEEE transactions on information theory*, 21-27.

Cover, T., & Hart, P. (1967). Nearest Neighbor Pattern Classification. *IEEE Transactions on Information Theory*, 21-27.

Cracknell, M. J. (2014). *Machine Learning for Geological Mapping: Algorithms and Applications.* Tasmania: Univesrity of Tasmania.

Cracknell, M. J., & Reading, A. M. (2014). Geological mapping using remote sensing data: A comparison of five machine learning algorithms, their response to variations in the spatial distribution of training data and the use of explicit spatial information. *Computers & Geosciences*, 22-33.

Cracknell, M. J., & Reading, A. M. (2014). *Unsupervised clustering of continental-scale geophysical and geochemical data using Self-Organising Maps*. Retrieved 10 24, 2017, from http://ecite.utas.edu.au/92286/1/2014_cracknell_reading_argaconf.pdf

Cracknell, M. J., Reading, A. M., & McNeill, A. W. (2013). Supervised and unsupervised classification of near-mine soil Geochemistry and Geophysics data. *Exploration Geophysics, 2013*(1), 1-4. Retrieved 10 24, 2017, from http://ecite.utas.edu.au/86778/1/86778 - supervised and unsupervised classification of near-mine soil geochemistry and geophysics data.pdf

D'Alessandro, A. B. (2015). Drones-New Technologies for Geophysics? *Near Surface Geoscience 2015-21st European Meeting of Environmental and Engineering Geophysics*.

Davis, J. C. (2011). *Statistics and Data Analysis.* New York: John Wiley & Sons.

Dietterich, T. (1995). Overfitting and undercomputing in machine learning. *27*(3), 326-327.

Eltner, A., Kaiser, A., Abellan, A., & Schindewolf, M. (2017). Time lapse structure-from-motion photogrammetry for continuous geomorphic monitoring: Time-lapse photogrammetry for continuous geomorphic monitoring. *Earth Surface Processes and Landforms*. Retrieved 9 17, 2017, from http://onlinelibrary.wiley.com/doi/10.1002/esp.4178/abstract

Escadafal, R. G. (1989). Munsell soil color and soil reflectance in the visible spectral bands of Landsat MSS and TM data. *Remote Sensing of Environment, 27*(1), 37-46.

Fayyad, U. M. (1995). *Studying the Sky/Planets Can Drown You in Images: Machine Learning Solutions at JPL/Caltech.* NASA.

G.H. Pettengill, P. F. (1991). Magellan: Radar Performance and Data Products. *Science*, pp. 252:260-265.

Gillan, J. K., Karl, J. W., Elaksher, A. F., & Duniway, M. C. (2017). Fine-Resolution Repeat Topographic Surveying of Dryland Landscapes Using UAS-Based Structure-from-Motion Photogrammetry: Assessing Accuracy and Precision against Traditional Ground-Based Erosion Measurements. *Remote Sensing, 9*(5), 437. Retrieved 9 17, 2017, from http://mdpi.com/2072-4292/9/5/437/notes

GitHub. (2017, September 21). Retrieved from https://github.com/tensorflow/tensorflow

Hastie, T. T. (2009). *Unsupervised learning.* New York: Springer.

Jonathan Huang, V. R. (2017, 06 15). *Google Research Blog*. Retrieved from Google Research Blog: https://research.googleblog.com/2017/06/supercharge-your-computer-vision-models.html

Kanevski, M. P. (2004). Environmental data mining and modeling based on machine learning algorithms and geostatistics. *Environmental Modelling & Software*, 845-855.

Kirkland, L. E., Herr, K. C., Salisbury, J. W., Keim, E. R., Adams, P. M., & Hackwell, J. A. (2002). *Infrared remote sensing of Mars and the Mars astrobiology exploration strategy*. Retrieved 10 21, 2017, from https://spiedigitallibrary.org/conference-proceedings-of-spie/4495/1/infrared-remote-sensing-of-mars-and-the-mars-astrobiology-exploration/10.1117/12.454754.full

Klaus Mangold, J. A. (2013). The physics of near-infrared photography. *European Journal of Physics*, S51-S71.

Krizhevsky, A. S. (2012). Imagenet classification with deep convolutional neural networks. *In Advances in neural information processing systems*, 1097-1105.

Kussul, N., Lavreniuk, M., Skakun, S., & Shelestov, A. (2017). Deep Learning Classification of Land Cover and Crop Types Using Remote Sensing Data. *IEEE GEOSCIENCE AND REMOTE SENSING LETTERS*, 778-782.

Langley, P., & Simon, H. A. (1995, November). Applications of machine learning and rule induction. *Communications of the ACM*, pp. 54-64.

LeCun, Y. (2017). *LeNet-5, convolutional neural networks*. Retrieved from http://yann.lecun.com/exdb/lenet/

Lucieer, A., Malenovský, Z., Veness, T., & Wallace, L. (2014). HyperUAS-Imaging Spectroscopy from a Multirotor Unmanned Aircraft System. *Journal of Field Robotics, 31*(4), 571-590. Retrieved 9 14, 2017, from http://doi.wiley.com/10.1002/rob.21508

Matsugu, M., Mori, K., Mitari, Y., & Kaneda, Y. (2003). Subject independent facial expression recognition with robust face detection using a convolutional neural network. *Neural Networks*, 555-559.

Morik, K. (1992). Morik, K. (1992). Applications of machine learning. *Current Developments in Knowledge Acquisition*, 9-13.

Nguyen, H. S., Skowron, A., & Szczuka, M. S. (2001). Analysis of Image Sequences for the Unmanned Aerial Vehicle. *Lecture Notes in Computer Science*, 333-338. Retrieved 9 17, 2017, from http://dl.acm.org/citation.cfm?id=665680

Özesmi, S. L., & Bauer, M. E. (2014). Satellite remote sensing of wetlands. *Wetlands Ecology and Management, 10*(5), 381-402. Retrieved 9 14, 2017, from https://link.springer.com/article/10.1023/a:1020908432489

Pavlis, T. L. (2011). Computer-based data acquisition and visualization systems in field geology: Results from 12 years of experimentation and future potential. *Geosphere*, 275-294.

Petropoulos, G. P., Arvanitis, K., & Sigrimis, N. (2012). Hyperion hyperspectral imagery analysis combined with machine learning classifiers for land use/cover mapping. *Expert Systems with Applications*, 3800-3809.

Pinheiro, P. O., & Collobert, R. (2015). From image-level to pixel-level labeling with convolutional networks. *In Proceedings of the IEEE Conference on Computer Vision and Pattern Recognition*, 1713-1721.

Pour, A. B. (2015). Hydrothermal alteration mapping from Landsat-8 data, Sar Cheshmeh copper mining district, south-eastern Islamic Republic of Iran. *Journal of Taibah University for Science, 9*(2), 155-166.

Proctor, J. &. (1975). The ecology of serpentine soils. *Advances in ecological research*, 255-366.

Qi, J., Lin, T., Zhao, T., Li, F., & Marfurt, K. (2016). Semisupervised multiattribute seismic facies analysis. *Interpretation*, 4(1).

Renguang, Z., & Carranza, E. (2011). Support vector machine: A tool for mapping mineral prospectivity. *Computers & Geosciences*, 1967-1975.

Richards, J. A. (2006). *Remote Sensing Digital Image Analisys.* Berlin: Springer.

scikit-learn developers. (2018, 09 20). *scikit-learn*. Retrieved from http://scikit-learn.org/stable/auto_examples/applications/plot_face_recognition.html

Shannon, W. M., Barens, C. G., & Bickford, M. (1997). Grenville Magmatism in West Texas: Petrology and Geochemistry of the Red Bluff Granitic Suite. *Journal of Petrology*, 1279-1305.

Sqalli, M. (2016, November 6). *Medium*. Retrieved from Medium: https://medium.com/@MSqalli/lane-detection-446986c44021

Swain, M. J., & Ballard, D. H. (1991, November). Color Indexing. *International Journal of Computer Vision, 7*(1), 11-32.

Talmage, D. A. (1986). Remote sensing using partially polarized light. *International Journal of Remote Sensing*, 47-64.

Turk, M. (1991). Face recognition using eigenfaces. *Computer Vision and Pattern Recognition*, 586-591.

Vapnik, V. N. (1998). *Statistical learning theory (Vol. 1).* New York: Wiley.

Vázquez-Tarrío, D. e. (2017). Using UAS optical imagery and SfM photogrammetry to characterize the surface grain size of gravel bars in a braided river (Vénéon River, French Alps). *Geomorphology, 285*, 94-105. Retrieved 9 17, 2017, from http://sciencedirect.com/science/article/pii/s0169555x16307590

Verhoeven, G. (2008). Imaging the invisible using modified digital still cameras for straightforward and low-cost archaeological near-infrared photography. *Journal of Archaeological Science*, 3087-3100.

Westoby, M. J. (2012). 'Structure-from-Motion'photogrammetry: A low-cost, effective tool for geoscience applications. *Geomorphology,* 300-314.

Young, H. D. (2004). *University physics with modern physics.*

Zhang, X. S. (2008). Enhancing photographs with near infra-red images. In Computer Vision and Pattern Recognition. *IEEE Conference*, 1-8.

VITA

Guillermo Vargas, a born and raised El Paso native, obtained his Bachelor of Science in Geology from the University of Texas at El Paso in December of 2014. Immediately after being awarded his degree, he applied to UTEP's graduate program in Geophysics where he focused on geophysics, UAVs and remote sensing. As a student, he also worked as a software engineer at Academic Technologies at UTEP where he built countless programs and apps for professors and students. He interned for Shell Oil developing machine learning solutions for seismic processing. He won the Southwest Section Imperial Barrel Award competition and started the first makerspace in El Paso called H3 Laboratories. An avid programmer, an eternal learner, enjoys conducting chemistry, electronics, and programming experiments at his home lab. In February of 2018 he became a father, adding to the list of things in his mind. He can't wait for his daughter to grow up and work with him on science experiments.

Guillermo earned his Master of Science in Geophysics in December 2018.

Contact Information: gavargas22@gmail.com

This thesis/dissertation was typed by Guillermo Vargas.